Spin-orbit torque induced dipole skyrmion motion at room temperature

Sergio A. Montoya,[1] Robert Tolley,[2,3] Ian Gilbert,[4] Soong-Geun Je,[5,6] Mi-Young Im,[5,6] and Eric E. Fullerton[2,3]
[1]*Space and Naval Warfare Systems Center Pacific, San Diego, California 92152, USA*
[2]*Center for Memory and Recording Research, University of California, La Jolla, California 92093, USA*
[3]*Department of Electrical and Computer Engineering, University of California, La Jolla, California 92093, USA*
[4]*Center for Nanoscale Science and Technology, National Institute of Standards and Technology, Gaithersburg, Maryland 20899, USA*
[5]*Center for X-Ray Optics, Lawrence Berkeley National Laboratory, Berkeley, California 94720, USA*
[6]*Department of Emerging Materials Science, Daegu Gyeongbuk Institute of Science and Technology, Daegu, Korea*

(Received 7 June 2018; revised manuscript received 3 August 2018; published 28 September 2018)

We demonstrate deterministic control of dipole-field-stabilized skyrmions by means of spin-orbit torques arising from heavy transition-metal seed layers. Experiments are performed on amorphous Fe/Gd multilayers that are patterned into wires and exhibit stripe domains and dipole skyrmions at room temperature. We show that while the domain walls and skyrmions are achiral on average due to lack of Dzyaloshinskii-Moriya interactions, the Néel-like closure domain walls at each surface are chiral and can couple to spin-orbit torques. The current-induced domain evolutions are reported for different magnetic phases, including disordered stripe domains, coexisting stripes and dipole skyrmions, and a close-packed dipole skyrmion lattice. The magnetic textures exhibit motion under current excitations with a current density $\sim 10^8$ A/m^2. By comparing the motion resulting from magnetic spin textures in Fe/Gd films with different heavy transition-metal interfaces, we confirm spin currents can be used to manipulate achiral dipole skyrmions via spin-orbit torques. We further show the current-induced response of a dipole skyrmion lattice where skyrmions move in channels between pinned regions.

DOI: 10.1103/PhysRevB.98.104432

I. INTRODUCTION

The ability to locally control magnetism through the use of electrical currents has led to the development of a range of new nonvolatile and efficient magnetism-based information technologies [1–3]. Current-induced magnetization dynamics were initially observed from spin-transfer torques in nanopillar devices with two magnetic layers [4–7]. The current becomes spin polarized by transmission through or upon reflection from the first magnetic layer and maintains this polarization as it passes through the nonmagnetic spacer and interacts with the second ferromagnetic layer. This interaction provides a torque on the magnetic driving precessions that can result in steady-state magnetic dynamics or magnetization reversal [7–10]. A similar phenomenon occurs in magnetic wires where spin current exerts a torque on the domain wall that enables their displacement in the electron flow direction [11–15].

The discovery of spin-orbit torques (SOTs) arising from current-induced spin accumulation at the interface between a ferromagnetic layer and a nonmagnetic layer with a large spin-orbit coupling (e.g., a heavy transition metal) provides an efficient method for manipulating spin structures within a single magnetic layer. The spin currents arise from the spin Hall effect in the nonmagnetic metal layer when a charge current flows within the sample plane. The spin Hall effect generates a spin current that flows vertically towards the ferromagnet. When this spin current is absorbed in the ferromagnetic it applies a SOT. This torque is particularly effective at moving chiral domain walls or skyrmions stabilized by interfacial Dzyaloshinskii-Moriya interaction (DMI) that arise at the magnetic-nonmagnetic interface. The direction of motion is set by the helicity of the spin structure and the sign of the spin Hall angle in the nonmagnetic layer. These observations demonstrated that magnetic spin textures could be displaced with low currents [16–26] in either patterned films [16–25] or continuous geometries [26]. These observations prompted research efforts to potentially develop next-generation high-efficiency and high-density information technologies in which individual skyrmions or chiral domain walls are used as logic and memory storage bits [27–31].

Thus far, the motion of chiral domain walls and skyrmions in thin films have been stabilized by interfacial DMI where the heavy-metal layer has the dual role of providing both the SOT and the DMI to stabilize the appropriate chiral spin structure. Here, we present direct observation of current-induced motion of magnetic stripe domains and dipole skyrmions in patterned wires of amorphous Fe/Gd multilayers at room temperature without the presence of DMI. The formation of sub-100-nm dipole-stabilized biskyrmions and skyrmions in this class of material were previously reported in Refs. [32] and [33], respectively. These magnetic textures result solely from the competition between magnetostatic and exchange energies [33] and there is no evidence of DMI in this system. Unlike skyrmions that form by means of DMI, a dipole skyrmion phase consists of an equal population of chiral cylindrical-like domains with two possible helicities [Figs. 1(a) and 1(b)] such that, on average, the material is achiral. This has been shown in Lorentz transmission electron microscopy which confirmed the dipole skyrmions possess a Bloch-like

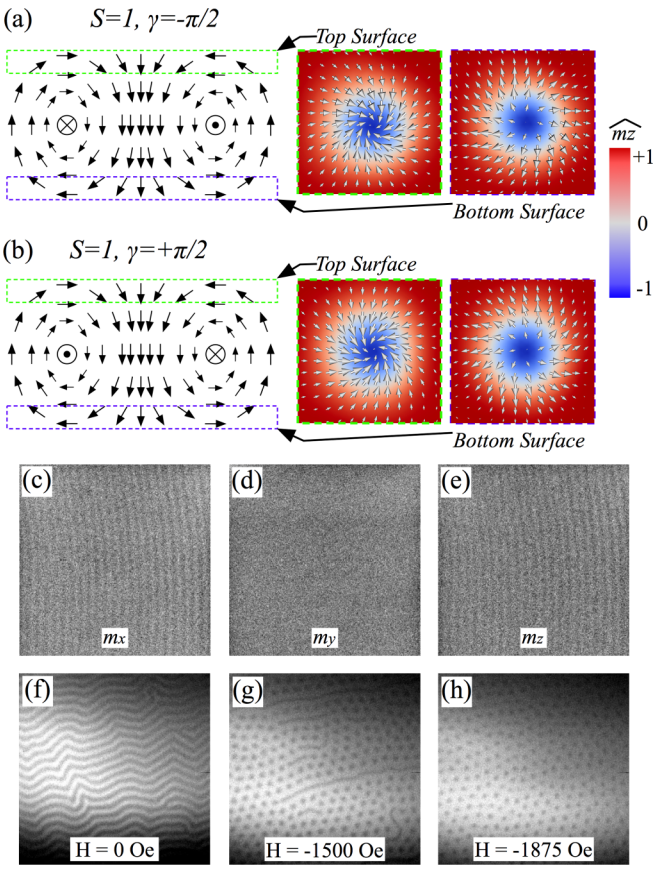

FIG. 1. Magnetic spin configuration of a dipole skyrmion with (a) clockwise and (b) counterclockwise helicity. (c–h) Domain morphology of Pt (5 nm)/[Fe (0.34 nm)/Gd (0.4 nm)]×100/Ta (3 nm) at room temperature. (c–e) SEMPA images detailing the surface magnetization (m_x, m_y, m_z) of the stripe domain phase at remanence. (f–h) Average-thickness perpendicular magnetization (m_z) field-dependent domain morphology obtained by soft-x-ray microscopy.

domain wall with equal population of two helicities for dipole-stabilized skyrmions in comparable Fe/Gd films [33].

In the currently studied Fe/Gd multilayer the thin-film shape anisotropy $2\pi M_S^2$ exceeds the uniaxial anisotropy K_U so the ratio $Q = K_U / 2\pi M_S^2 < 1$ [34], and the dipole skyrmion phase becomes favorable for relatively thick magnetic films. For such films, numerical simulations predicted that dipole skyrmions possess a domain wall that is Bloch-like at the center of the film but broadens and transitions to Néel-like walls towards the film surface [Figs. 1(a) and 1(b)] which are often referred to as closure domains or Néel caps [35]. While the Bloch nature of the wall in the center of the film will have one or two possible helicities shown in Figs. 1(a) and 1(b), the Néel-wall structure of the spins near the surfaces of the film have the same helicity for the top surface and the opposite helicity at the bottom surface (thus in total the spin structure is achiral). For the examples shown in Figs. 1(a) and 1(b) the magnetic spins at the top surface point inwards into the skyrmion whereas at the bottom surface they point outwards from the dipole skyrmion and this is independent of the helicity of the Bloch wall in the core. The chiral nature of the surface spins in closure domains, even in the absence of DMI, has previously been shown by x-ray resonant magnetic scattering from stripe domains using circularly polarized soft x rays [36] and has been recently observed in chiral magnetic spin textures stabilized by DMI in bulk magnets [37] and thin-film heterostructures [38–40]. Here, we demonstrate that SOTs can be used to manipulate dipole skyrmions, by interfacing the dipole-stabilized chiral surface spin structures of Fe/Gd films with heavy transition-metal layers (e.g., Pt and Ta). Our results show the current-driven motion of dipole skyrmions depends, as expected, on the sign of the spin Hall angle of the transition-metal layer and the chirality of the near-surface region of the stripe domains and dipole skyrmions.

II. EXPERIMENTAL METHODS AND RESULTS

The amorphous $[\mathrm{Fe}(0.34\,\mathrm{nm})/\mathrm{Gd}(0.4\,\mathrm{nm})]_N$ multilayer films were fabricated by magnetron sputtering at room temperature in a 3-mTorr Ar pressure. The chamber base pressure was $<3 \times 10^{-8}$ Torr. The multilayer films were grown by alternatively depositing Fe and Gd layers for N repetitions with different seed and capping layers. The Fe and Gd layer thickness values were optimized to achieve the skyrmion phase at room temperature [33]. Selected Fe/Gd films were deposited onto photolithographic defined wires on 100-nm-thick SiN membranes with 5 × 5-mm frames and 1 × 1-mm windows. Transition-metal Pt and Ta seed and capping layers were used to protect the specimen from corrosion. Fe/Gd full films were also deposited onto Si substrate with a native-oxide layer for magnetometry measurements and SiN membranes to serve as reference samples.

III. DOMAIN MORPHOLOGY OF Fe/Gd PATTERNED WIRES

The magnetic domains at remanence were imaged using scanning electron microscopy with polarization analysis (SEMPA) at the National Institute of Standards and Technology in Gaithersburg, Maryland. The field-dependent magnetic domains in patterned wires were imaged using full-field soft-x-ray transmission microscopy at Lawrence Berkeley National Laboratory, Advanced Light Source, Beamline 6.1.2 along the Fe L_3 (708-eV) absorption edge. Figures 1(c)–1(e) show SEMPA images of the stripe domains in remanence. This technique is surface sensitive and can image the projection of the magnetic spin x, y, and z directions. Figures 1(c)–1(e) detail the surface (m_x, m_y, m_z) magnetization distributions, where the perpendicular stripe domains with opposite orientation are represented along the (m_z) magnetization as dark/light contrast, whereas the Néel closure domains are solely seen by the periodic (m_x) magnetization consistent with the schematic in Figs. 1(a) and 1(b). No contrast is observed along the m_y direction, as expected for vertically oriented stripe domains. This clearly shows the expected closure domain structure for the stripe phase. Because this imaging technique is sensitive to external magnetic fields we cannot image the surface domain structure in an applied field.

The field-dependent domain morphology and its current-induced motion were studied using full-field transmission soft-x-ray microscopy measured at the Fe L_3 (708-eV) absorption edge in 10-μm-wide and 5-mm-long Fe/Gd patterned wires (see Methods, for further details). Figures 1(f)–1(h) show the domain morphology of the Pt (5 nm)/[Fe (0.34 nm)/Gd (0.4 nm)]×100/Ta (3 nm) wire sample imaged while a perpendicular magnetic field was applied from negative to positive magnetic saturation. Each image details the perpendicular magnetization averaged over the thickness of the film. At remanence [Fig. 1(f)], the film exhibits stripe domains with a stripe periodicity of 180 nm consistent with Fig. 1(c) imaged for a full film. The stripe domains are preferentially aligned in the direction of the Fe/Gd wire length. Under a perpendicular field, we observed first coexisting stripe domains and dipole skyrmions [Fig. 1(g)] and then a close-packed lattice of dipole skyrmions [Fig. 1(h)] which is similar to the results of Ref. [33]. The dipole skyrmion features are 90 nm in diameter at $H_z = +2000$ Oe. Limitations in the applied magnetic field did not allow the observation of the disordered dipole skyrmion phase and saturation, as previously reported in Ref. [33]. The saturation field for this Fe/Gd wire exists above $H_z > 2800$ Oe, which is above the maximum applied magnetic field of the microscope.

IV. CURRENT-INDUCED DYNAMICS OF STRIPE DOMAINS AND DIPOLE SKYRMIONS

We applied current pulses to the wire samples and imaged the evolution of domain structure under current. The domain morphology at any given field was recorded prior to the application of an electrical current pulse. For the measurements presented, we used 10-ms-long current pulse with amplitude up to $j = 5 \times 10^8$ A/m^2. After the current excitation pulse, the domain morphology was again recorded. This process was repeated until collecting several frames. Afterwards, the magnetic field history was cycled (e.g., the magnetic field was increased to magnetic saturation and then the field was reduced to the opposite magnetic saturation field, prior to returning to the desired magnetic field). In order to clearly identify current-induced motion of magnetic textures, an area of the wire with a defect within the field of view was chosen to facilitate alignment between image snapshots. Each snapshot results from a 2-s exposure and five averages.

Figure 2(a) shows the domain morphology of coexisting stripe domains and dipole skyrmions that form in Pt (5 nm)/[Fe (0.34 nm)/Gd (0.4 nm)] ×100/Ta (3 nm) film under a perpendicular field of $H_z = +1250$ Oe. We applied a series of 10-ms-long current pulses with density amplitude of $j = 5 \times 10^8$ A/m^2. We generally observe that the first current pulse alters the domain structures (e.g., converting stripes into skyrmions) and then subsequent current pulses induce directional motion of the domains. Figures 2(b)–2(d) show a sequence of snapshots of the evolution of the domain states when these are subjected to a sequence of single current pulses. Depending on the current pulse iteration, denoted p_1, p_2, and p_3 in Figs. 2(a)–2(d), we find there is a mixture of pinned and moving dipole skyrmions. By tracking the current-induced motion of dipole skyrmions, we observe these textures move in the direction of the current flow.

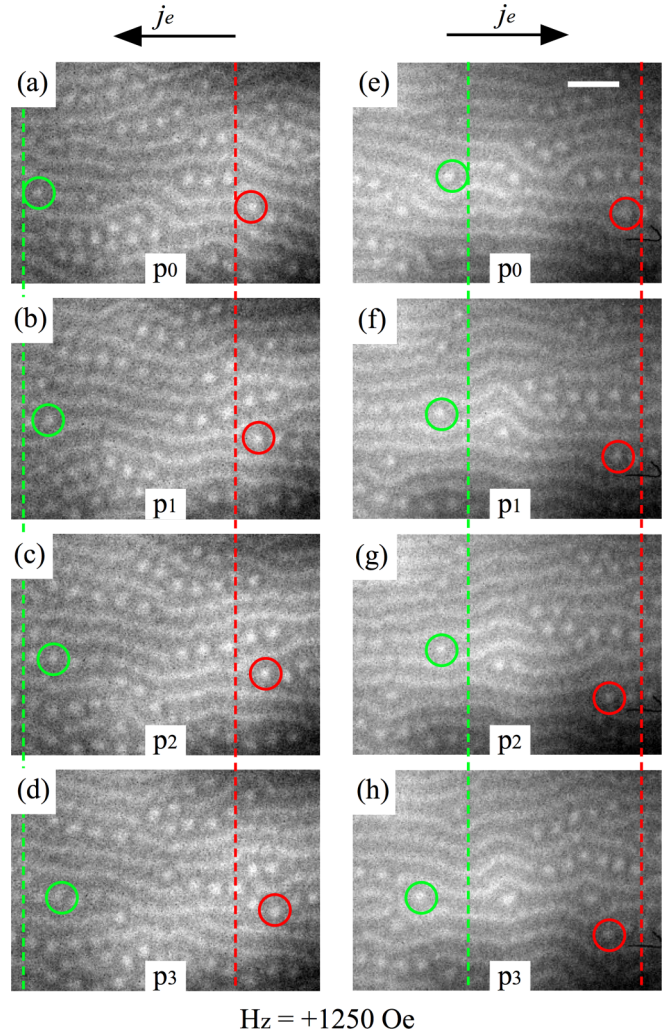

FIG. 2. Current induced motion observed in coexisting stripe and dipole skyrmion magnetic phase in Pt (5 nm)/[Fe (0.34 nm)/Gd (0.4 nm)] ×100/Ta (3 nm) at room temperature under a perpendicular magnetic field of $H_z = +1250$ Oe. The images showing the domain morphology are acquired with soft-x-ray microscopy. (a–d) Domain motion that results from applying a positive polarity current, where panel (a) shows the domain state prior to the current pulse and panels (b)–(d) show domain states after three iterative current pulses. (e, f) Detail current-driven domain motion for a negative polarity current. Dipole skyrmions are outlined to serve as a guide to the eye to track their motion and the electron flow direction is labeled for both cases. The scale bar in panel (a) corresponds to 1 μm.

Example dipole skyrmions that are continuously displaced under the application of the current pulses have been outlined in Figs. 2(a)–2(d). When the electrical current is reversed [Figs. 2(e)–2(h)], we observe the dipole skyrmions move opposite to the original direction and again along the current flow direction. Since the motion is along the current flow direction we attribute the motion to SOTs from the Pt seed layer acting on the chiral spin structure at the bottom interface, and the direction of propagation is consistent with the results of Ref. [17]. The top Ta layer is thinner and partially oxidizes and therefore we expect it to contribute far less to the domain motion.

To further probe the driving mechanism that results in current-motion of dipole skyrmions, we have also studied the current dynamics for a Ta (5 nm)/[Fe (0.34 nm)/Gd (0.4 nm)]×100/Pt (3 nm) film (Fig. 3) where the materials of the seed and capping layers are inverted. Since heavy transition metals Pt and Ta have opposite sign of the spin Hall angle [41,42], we expect the motion of dipole skyrmions with respect to the current flow to be reversed if the SOT is the driving mechanism. Figure 3(a) shows the domain morphology, primarily consisting of stripe domains and a few dipole skyrmions when the film is exposed to a magnetic field of $H_z = -875$ Oe [Fig. 3(a)]. After the first current pulse, most of the stripe domains collapse into a collection of dipole skyrmions that occupy the region previously filled by the original stripe domain [Fig. 3(b)]. In the previous magnetic film (Fig. 2) there was limited evidence of stripe domains collapsing into dipole skyrmions. As discussed in Ref. [33], we find that dipole skyrmions can form by two mechanisms: (i) the extremities of a single stripe domain can collapse to form a dipole skyrmion, or (ii) a single stripe domain can pinch into a line of dipole skyrmions where the stripe domain previously existed. Both these mechanisms were previously observed in Fe/Gd films [33] and appear to be favored under different ratios of magnetic energies suggesting these Fe/Gd wires possess small differences in magnetic properties for different seed layers. Figures 3(b)–3(e) detail subsequent snapshots of the domain morphology after iterative single electrical pulse excitations. Once the film primarily consists of dipole skyrmions, the current-driven stripe to dipole skyrmion transformation is no longer predominant. After the first pulse there is a mixture of pinned and moving dipole skyrmions; however, the displacement of dipole skyrmions is now in the direction of the electron flow [Figs. 3(b)–3(e)]. Examples of moving dipole skyrmions have been outlined in Figs. 3(a)–3(e). When the magnetic field is reversed, $H_z = +875$ Oe, we observe comparable current-induced dynamics of the magnetic textures as outlined for $H_z = -875$ Oe, and dipole skyrmions again displace along the electron flow [Figs. 3(f)–3(j)]. As discussed below, this is expected as the chirality of the surface closure domains remains the same after inverting the field. Further imaging of stripe domain response to current pulses including current induced stripe-to-skyrmion generation is shown in Supplemental Material Secs. 1 and 2 [43].

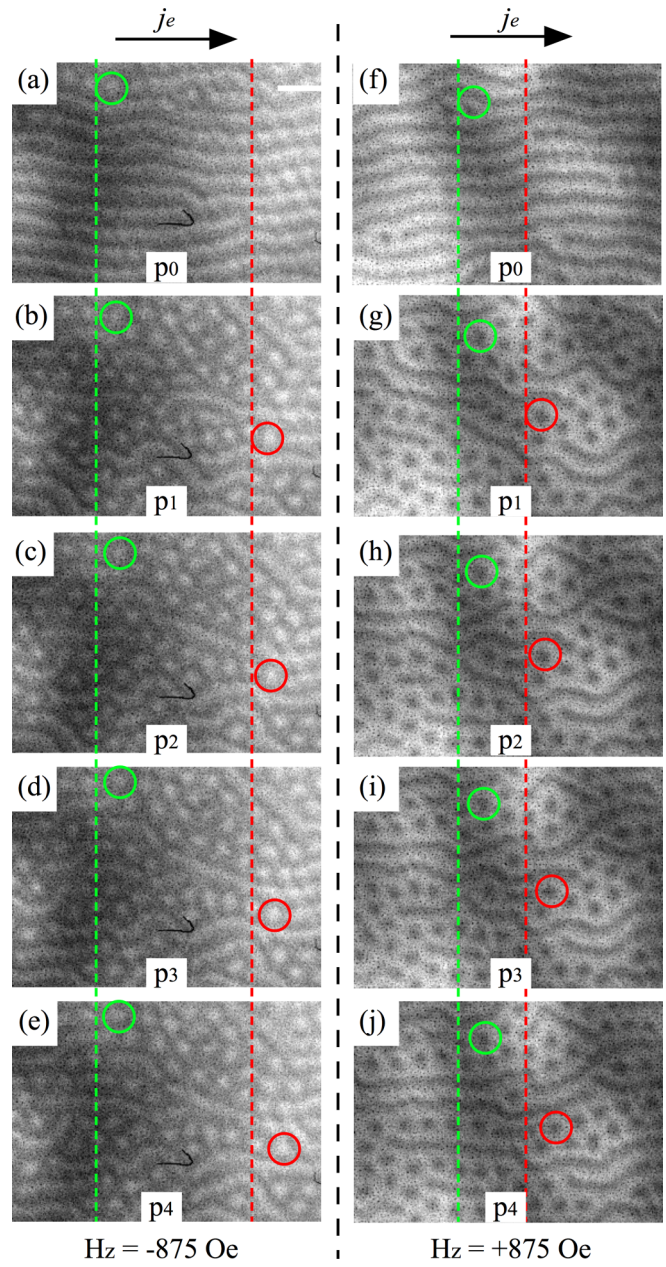

FIG. 3. Current induced motion observed in coexisting stripe and dipole skyrmion magnetic phase in Ta (5 nm)/[Fe (0.34 nm)/Gd (0.4 nm)] ×100/Pt (3 nm) at room temperature when exposed to a negative polarity current pulse. The images showing the domain morphology are acquired with soft-x-ray microscopy. (a–e) Domain motion of magnetic states that exist under a perpendicular magnetic field of $H_z = -875$ Oe, where panel (a) shows the domain state prior to the current pulse and panels (b)–(e) show domain states after three iterative current pulses. (f–j) Domain motion of magnetic states under $H_z = +875$ Oe, where panel (f) shows the domain state prior to the current pulse and panels (g)–(j) show domain states after three iterative current pulses. Dipole skyrmions are outlined to serve as a guide to the eye to track their motion. The scale bar in panel (a) corresponds to 1 μm.

V. CURRENT-INDUCED MOTION IN A DIPOLE SKYRMION LATTICE

We also investigated the current-induced dynamics that results from a close-packed lattice of dipole skyrmions using current pulse excitations. Figure 4 shows the domain morphology of Ta (5 nm)/[Fe (0.34 nm)/Gd (0.4 nm)] ×100 /Pt (3 nm) that forms under a perpendicular magnetic field of $H_z = -2250$ Oe [Fig. 4(a)]. The dipole skyrmion features are 85 nm in diameter and arrange in a disordered close-packed array. When a current pulse is injected, complex motion is observed throughout the field of view (see Supplemental Material [44]). It is difficult to track individual dipole skyrmions by comparing before/after static images because these textures are arranged in a close-packed lattice making the identification of individual skyrmions difficult. To illustrate dipole skyrmion motion, we have processed the raw images, such as the one shown in Fig. 4(a), to remove the background

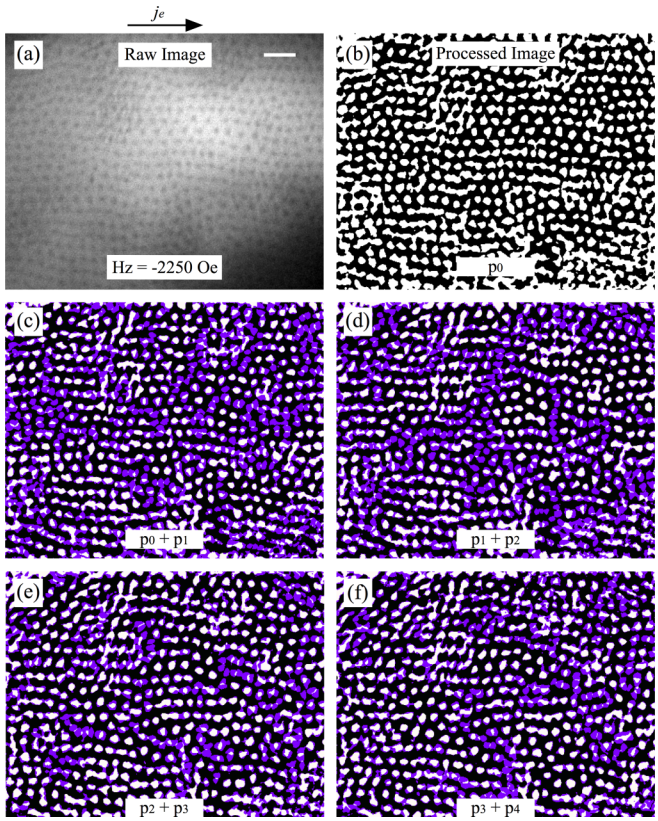

FIG. 4. Current induced motion of dipole skyrmions arranged in a close-packed lattice in Ta (5 nm)/[Fe (0.34 nm)/Gd (0.4 nm)]×100/Pt (3 nm) at room temperature. (a) Soft-x-ray microscopy image showing the domain morphology that is obtained under the application of a negative perpendicular magnetic field, $H_z = -2250$ Oe. (b) Postprocessed binary image detailing the domain morphology shown in panel (a) with background subtracted. (c, d) The dynamics of close-packed dipole skyrmions that result from injecting four consecutive negative polarity current pulses. Each frame details the sum of the images detailing the domain morphology before and after the injecting of the current pulse. The purple colored regions detail regions where changes have occurred in the domain morphology after the current pulse was applied. The scale bar in panel (a) corresponds to 1 μm.

and construct binary images. Figure 4(b) shows the postprocessed image that was obtained from Fig. 4(a) where the white regions are the skyrmions. Changes in the domain morphology with current pulses are outlined as contrast changes that result from the summation of binary images obtained before/after a current pulse is applied. Figures 4(c)–4(f) show the domain motion that results from four iterative single current pulses where the skyrmions that are pinned appear as white domains in the summation (i.e., did not move under current) and skyrmions that move will yield an intermediate contrast. We observe there are regions of pinned dipole skyrmions coexisting with moving dipole skyrmions. The displacements of dipole skyrmions are in the form of riverlike channels that are oriented at various angles relative to the electron flow. By inspecting the snapshots of the domain morphology [Figs. 4(c)–4(f)] we are able to track the skyrmion positions and determine an average skyrmion speed $\langle s \rangle = 6$ μm/s when exposed to a single current pulse.

Figure 5 shows the current-induced dynamics of a close-packed lattice of dipole skyrmions under the application of a single current pulse with different current density amplitude which reveal the transition from the pinned to creep regime. To highlight the motion of the skyrmions the domain images are converted into binary images as described earlier. After a series of current pulses are injected, at a current density amplitude, the domain morphology is reset by cycling the perpendicular field up to positive saturation, then reducing the field to negative saturation, and finally increasing the field up to $H_z = +2000$ Oe under which a close-packed lattice of dipole skyrmions forms. We observe the transition from the pinned to creep regime with increasing current density amplitudes from $j = 0.5 \times 10^8$ to 5×10^8 A/m^2 (Fig. 5). Current amplitudes below $j < 3 \times 10^8$ A/m^2 exert a weak SOT that is unable to displace the textures from their pinning site. Figures 5(a)–5(c) show the domain states after the injection of three iterative current pulses with amplitude $j = 0.5 \times 10^8$ A/m^2, where there is evidence of minor changes in contrast around many of the individual textures. The latter results from illumination artifacts when recording domain morphology snapshots. Increasing the current density amplitude, $j > 3 \times 10^8$ A/m^2, we observe a number of dipole skyrmions exhibiting motion increases from a few clustered textures in scattered regions across the field of view to many textures that form riverlike channels [Figs. 5(d)–5(l)].

VI. DISCUSSION

Since the closure domains of dipole skyrmions possess an opposite Néel-like chiral structure on the top and bottom surface [Figs. 1(a) and 1(b)] and heavy transition-metal interfaces with different spin Hall angle, we can expect the coupling to spin currents will be asymmetric at the top and bottom surface. The latter results in a dipole skyrmion experiencing an opposite SOT at each surface. Since the SOT depends on the spin Hall angle [41,42] and thickness [45,46] of the heavy transition metal, we expect the force amplitude is different at both surfaces. Since the observed directions of the skyrmion motion can be explained by the combination of chirality of the Néel caps and the SOT at the bottom surface, we conclude that the SOT arising from the thicker seed layer plays a dominant role in the motion of dipole skyrmions. Results in Figs. 2 and 3 show there is a dependence in the direction of dipole skyrmion motion relative to inverting the seed/capping layers. A more efficient displacement of dipole skyrmions will likely result when using the same heavy transition metal at both surfaces, as well as reducing the total thickness of the magnetic specimen such that the SOT efficiency increases [47]. Also motion of skyrmions would be more efficient if we could image at higher fields where individual skyrmions can be isolated. In the present experiments we have close-packed domain structures so stripe-skyrmion or skyrmion-skyrmion interaction limits the mobility, giving the relatively low velocities observed. Finally, we note that evidence of SOTs driving the motion of dipole skyrmions

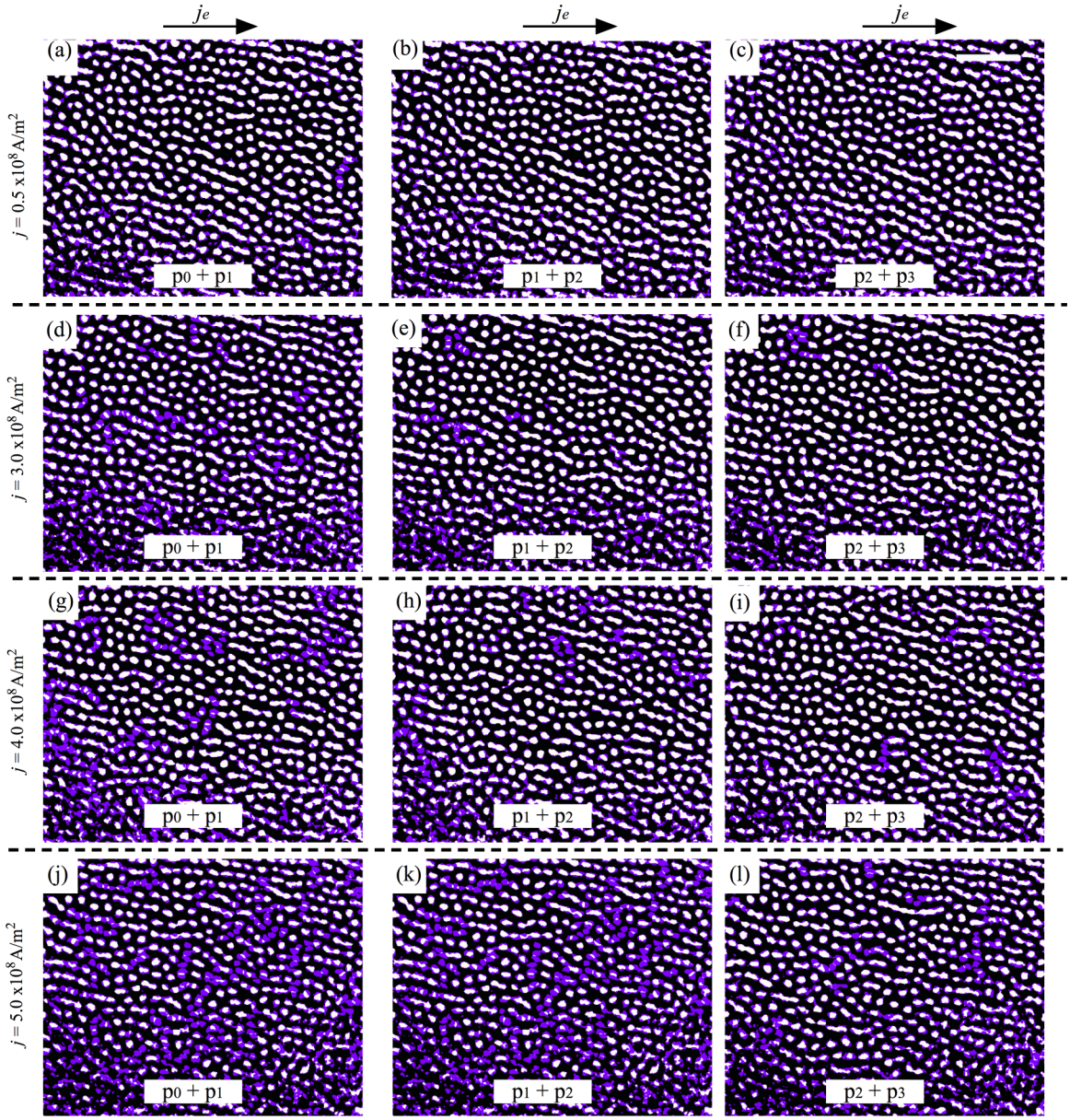

FIG. 5. Current-induced motion of dipole skyrmions arranged in a close-packed lattice in Ta (5 nm)/[Fe (0.34 nm)/Gd (0.4 nm)]×100/Pt (3 nm) at room temperature. Each frame shows the sum of the binary images detailing the domain morphology before/after injecting current pulse excitations with different current density amplitude: (a–c) $j = 0.5 \times 10^8$ A/m^2, (d–f) $j = 3 \times 10^8$ A/m^2, (g–i)$j = 4 \times 10^8$ A/m^2, and (j–l) $j = 5 \times 10^8$ A/m^2. At each current density, the dynamics are captured for three consecutive current pulses. The purple colored regions show areas where changes have occurred after the injection of a current pulse. The scale bar in panel (c) corresponds to 1 μm.

is also supported by the observation of stripe-to-skyrmion generation [48].

Our results on the current-induced motion in the skyrmion lattice phase are similar to a recent numerical study of skyrmion lattices in the presence of disorder [49]. Using a particle-based model of a modified Thiele equation, these authors predicted the skyrmion Hall effect depends on the drive force acting on the skyrmions as well as the pinning force that arises from defects. The paper anticipates that (i) under weak drive forces the skyrmion Hall angle is not constant and skyrmion motion is oriented in scattered directions; (ii) increasing the drive force acting on the skyrmions, median drive force, results in the riverlike motion that is oriented at an angle relative to the direction of the drive force; and (iii) only after a sufficiently high drive force is applied do all the skyrmion domains move uniformly along the skyrmion Hall angle. In our Fe/Gd films, we appear, within the context of this model, to be inducing dipole skyrmion motion in the creep regime under a median drive force. We find that reducing the current pulse amplitude to $j = 3 \times 10^8$ A/m^2 results in motion of clustered dipole skyrmions in random regions within the field of view, as numerically predicted by

Ref. [49] under the application of a weak drive force. Because of instrumentation limitations, we were unable to inject higher amplitude current pulses (e.g., the high drive force regime) to observe dipole skyrmion motion in the flow regime. We expect that skyrmion Hall effect [28,50–52] would be manifested by dipole skyrmions in the flow regime, such that dipole skyrmions with clockwise [Fig. 1(a)] and counterclockwise [Fig. 1(b)] Bloch helicity components would displace tangentially in the same direction [53–56] based on their common topological charge; however, in the case of a dampinglike SOT the mixed chirality can play a role in the experimentally measured skyrmion Hall angle [56].

In conclusion we demonstrated that sub-100-nm dipole skyrmions can be manipulated with spin currents via spin-orbit torque. We have experimentally verified the presence of closure domains in our Fe/Gd films which supports the numerically predicted spin structure of dipole skyrmions that form in magnets with a Q factor < 1. The observation of complex and nontrivial current dynamics resulting from a large ensemble of magnetic spin textures illustrates the importance of understanding pinning and repulsive forces. The ability to manipulate dipole skyrmions with spin currents encourages potential implementation into spintronic based devices and sensors.

ACKNOWLEDGMENTS

Work at Space and Naval Warfare Systems Center Pacific including nanofabrication and participation at synchrotron experiments was supported by the Naval Innovation Science and Engineering Program. Work at University of California San Diego including sample growth and materials characterization and participation in synchrotron experiments was supported by US Department of Energy, Office of Basic Energy Sciences (Grant No. DE-SC0003678). Work at the Advanced Light Source was supported by the US Department of Energy (Grant No. DE-AC02-05CH11231). Work at the National Institute of Standards and Technology's Center for Nanoscale Science and Technology was performed under Project No. R13.0004.04. I.G. acknowledges support from the National Research Council's Research Associateship Program. M.-Y. Im acknowledges support by the Leading Foreign Research Institute Recruitment Program through the National Research Foundation (NRF) of Korea funded by the Ministry of Education, Science and Technology (MEST) (Grant No. 2012K1A4A3053565) and by the DGIST Research and Development program of the Ministry of Science, Information and Communications Technology (ICT) and Future Planning (Grant No. 18-BT-02).

[1] C. Chappert, A. Fert, and F. N. Van Dau, The emergence of spin electronics in data storage, Nat. Mater. **6**, 813 (2007).
[2] J. A. Katine and E. E. Fullerton, Device implications of spin-transfer torques, J. Magn. Magn. Mater. **320**, 1217 (2008).
[3] H. Ohno, Md. D. Stiles, and B. Dieny, Spintronics, in *Proceedings of IEEE*, Vol. 104 (IEEE, Piscataway, NJ, 2016), pp. 1782–1786.
[4] S. I. Kiselev *et al.*, Microwave oscillations of a nanomagnet driven by a spin-polarized current, Nature (London) **425**, 380 (2003).
[5] S. Ikeda *et al.*, Magnetic tunnel junctions for spintronic memories and beyond, IEEE Trans. Electron Devices **54**, 991 (2007).
[6] Z. Diao *et al.*, Spin transfer switching in dual MgO magnetic tunnel junctions, Appl. Phys. Lett. **90**, 132508 (2007).
[7] E. B. Myers, D. C. Ralph, J. A. Katine, R. N. Louie, and R. A. Buhrman, Current-induced switching of domains in magnetic multilayer devices, Science **285**, 867 (1999).
[8] J. C. Slonczewski, Current-driven excitation of magnetic multilayers, J. Magn. Magn. Mater. **159**, L1 (1996).
[9] L. Berger, Emission of spin waves by a magnetic multilayer traversed by a current, Phys. Rev. B **54**, 9353 (1996).
[10] M. Tsoi, A. G. M. Jansen, J. Bass, W.-C. Chiang, M. Seck, V. Tsoi, and P. Wyder, Excitation of a Magnetic Multilayer by an Electric Current, Phys. Rev. Lett. **80**, 4281 (1998).
[11] E. Salhi and L. Berger, Current-induced displacements and precession of a Bloch wall in Ni-Fe thin films, J. Appl. Phys. **73**, 6405 (1993).
[12] L. Gan, S. H. Chung, K. H. Aschenbach, M. Dreyer, and R. D. Gomez, Pulsed-current-induced domain wall propagation in Permalloy patterns observed using magnetic force microscopy, IEEE Trans. Magn. **36**, 3047 (2000).
[13] D. Atkinson *et al.*, Magnetic domain-wall dynamics in submicrometer ferromagnetic structure, Nat. Mater. **2**, 85 (2003).
[14] A. Yamaguchi, T. Ono, S. Nasu, K. Miyake, and T. Shinjo, Real-Space Observation of Current-Driven Domain Wall Motion in Submicron Magnetic Wires, Phys. Rev. Lett. **92**, 077205 (2004).
[15] S. P. Parkin, M. Hayashi, and L. Thomas, Magnetic domain-wall racetrack memory, Science **320**, 190 (2008).
[16] K.-S. Ryu, L. Thomas, S.-H. Yang, and S. P. Parkin, Chiral spin torque at magnetic domain, Nat. Nanotech. **8**, 527 (2013).
[17] S. Emori, U. Bauer, S.-M. Ahn, E. Martinez, and G. D. Beach, Current-driven dynamics of chiral ferromagnetic domain walls, Nat. Mater. **12**, 611 (2013).
[18] A. V. Khvalkovskiy, V. Cros, D. Apalkov, V. Nikitin, M. Krounbi, K. A. Zvezdin, A. Anane, J. Grollier, and A. Fert, Matching domain-wall configuration and spin-orbit torque for efficient domain-wall motion, Phys. Rev. B **87**, 020402(R) (2013).
[19] S.-H. Yang, K.-S. Ryu, and S. P. Parkin, Domain-wall velocities of up to 750 m/s driven by exchange coupling torque in synthetic antiferromagnets, Nature Nanotech. **10**, 221 (2015).
[20] W. Jiang *et al.*, Blowing magnetic skyrmion bubbles, Science **349**, 283 (2015).
[21] W. Jiang *et al.*, Mobile Néel skyrmions at room temperature: Status and future, AIP Adv. **6**, 055602 (2016).
[22] R. Tolley, S. A. Montoya, and E. E. Fullerton, Room-temperature observation and current control of skyrmions in Pt/Co/Os/Pt thin films, Phys. Rev. Materials **2**, 044404 (2018).
[23] S. Woo *et al.*, Spin-orbit torque-driven skyrmion dynamics revealed by time-resolved x-ray microscopy, Nat. Commun. **8**, 15573 (2017).
[24] W. Legrand *et al.*, Room temperature current-induced generation and motion of sub-100nm skyrmions, Nano Lett. **17**, 2703 (2017).
[25] A. Hrabec *et al.*, Current-induced skyrmion generation and dynamics in symmetric bilayers, Nat. Commun. **8**, 15765 (2017).

[26] G. Yu *et al.*, Room-temperature creation, and spin-orbit torque manipulation of skyrmion in thin films with engineered asymmetry, Nano. Lett. **16**, 1981 (2016).
[27] A. Fert, V. Cros, and J. Sampaio, Skyrmions on track, Nature Nanotech. **8**, 152 (2013).
[28] J. Iwasaki, M. Mochizuki, and N. Nagaosa, Universal current-velocity relation of skyrmion motion in chiral magnets, Nat. Commun. **4**, 1463 (2013).
[29] R. Tomasello *et al.*, A strategy for the design of skyrmion racetrack memories, Sci. Rep. **4**, 6784 (2014).
[30] X. Zhang, M. Ezawa, and Y. Zhou, Magnetic skyrmion logic gates: Conversion, duplication and merging of skyrmions, Sci. Rep. **5**, 9400 (2015).
[31] W. Koshibae *et al.*, Memory functions of magnetic skyrmions, Jpn. J. Appl. Phys. **54**, 053001 (2015).
[32] J. C. T. Lee *et al.*, Synthesizing skyrmion bound pairs in Fe-Gd thin films, Appl. Phys. Lett. **109**, 022402 (2016).
[33] S. A. Montoya *et al.*, Tailoring the magnetic energies to form dipole skyrmions and dipole skyrmion lattices, Phys. Rev. B **95**, 024415 (2017).
[34] C. Kooy and U. Enz, Experimental and theoretical study of the domain configuration in thin layers of $BaFe_{12}O_{19}$, Philips Res. Rep. **15**, 7 (1960).
[35] A. Hubert and R. Schäfer, *Magnetic Domains* (Springer, Berlin, 1998), pp. 315–319.
[36] H. A. Dürr *et al.*, Chiral magnetic domain structures in ultrathin FePd films, Science **284**, 2166 (1999).
[37] S. Zhanga *et al.*, Reciprocal space tomography of 3D skyrmion lattice order in chiral magnet, Proc. Natl. Acad. Sci. USA **115**, 6386 (2018).
[38] J.-Y. Chauleau, W. Legrand, N. Reyren, D. Maccariello, S. Collin, H. Popescu, K. Bouzehouane, V. Cros, N. Jaouen, and A. Fert, Chirality in Magnetic Multilayers Probed by the Symmetry and the Amplitude of Dichroism in X-Ray Resonant Magnetic Scattering, Phys. Rev. Lett. **120**, 037202 (2018).
[39] W. Legrand *et al.*, Hybrid chiral domain walls and skyrmions in magnetic multilayers, Sci. Adv. **4**, eaat0415 (2018).
[40] Y. Dovzhenko *et al.*, Magnetostatic twists in room-temperature skyrmions explored by nitrogen-vacancy center spin texture reconstruction, Nat. Commun. **9**, 2712 (2018).
[41] L. Liu, O. J. Lee, T. J. Gudmundsen, D. C. Ralph, and R. A. Buhrman, Current-Induced Switching of Perpendicularly Magnetized Magnetic Layers Using Spin Torque from the Spin Hall Effect, Phys. Rev. Lett. **109**, 096602 (2012).
[42] L. Liu, C.-F. Pai, Y. Li, H. W. Tseng, T. J. Ralph, and R. A. Buhrman, Spin-torque switching with the giant spin hall effect of tantalum, Science **336**, 555 (2012).
[43] See Supplemental Material at http://link.aps.org/supplemental/10.1103/PhysRevB.98.104432 for (1) current-induced dynamics of stripe domains at remanence and (2) the current-induced stripe to dipole skyrmion generation.
[44] See Supplemental Material at http://link.aps.org/supplemental/10.1103/PhysRevB.98.104432 for video detailing the current-induced motion of a close-packed lattice of dipole skyrmions.
[45] J. Kim *et al.*, Layer thickness dependence of the current-induced effective field vector in Ta|CoFeB|MgO, Nat. Mater. **12**, 240 (2013).
[46] Y. Wang, P. Deorani, X. Qiu, J.-H. Kwon, and H. Yang, Determination of intrinsic spin Hall angle in Pt, Appl. Phys. Lett. **105**, 152412 (2014).
[47] C.-F. Pai, Y. Ou, L. H. Vilela-Leão, D. C. Ralph, and R. A. Buhrman, Dependence of the efficiency of spin Hall torque on the transparency of Pt/ferromagnetic layer interfaces, Phys. Rev. B **92**, 064426 (2015).
[48] S.-Z. Lin, Edge instability in a chiral stripe domain under an electric current and skyrmion generation, Phys. Rev. B **94**, 020402(R) (2016).
[49] C. Reichhardt and C. J. O. Reichhardt, Noise fluctuations and drive dependence of the skyrmion Hall effect in disordered systems, New J. Phys. **18**, 095005 (2016).
[50] N. Nagaosa and Y. Tokura, Topological properties and dynamics of magnetic skyrmions, Nature Nanotechnol. **8**, 899 (2013).
[51] J. Sampaio, V. Cros, S. Rohart, A. Thiaville, and A. Fert, Nucleation, stability and current-induced motion of isolated magnetic skyrmions in nanostructures, Nature Nanotech. **8**, 839 (2013).
[52] W. Jiang *et al.*, Direct observation of the skyrmion hall effect, Nat. Phys. **13**, 162 (2017).
[53] A. P. Malozemoff, Mobility of bubbles with small numbers of Bloch lines, J. Appl. Phys. **44**, 5080 (1973).
[54] C. Reichhardt, D. Ray, and C. J. O. Reichhardt, Quantized transport for a skyrmion moving on a two-dimensional periodic substrate, Phys. Rev. B **91**, 104426 (2015).
[55] S. S.-L. Zhang and O. Heinonen, Topological Hall effect in diffusive ferromagnetic thin films with spin flip scattering, Phys. Rev. B **97**, 134401 (2018).
[56] F. Büttner, I. Lemesh, and G. S. D. Beach, Theory of isolated magnetic skyrmions: From fundamentals to room temperature applications, Sci. Rep. **8**, 4464 (2018).